J. Plasma Physics (2013), vol. 79, part 5, pp. 973–979. © Cambridge University Press 2013
doi:10.1017/S0022377813000809

Plasmons carrying orbital angular momentum in quantum plasmas

SHABBIR A. KHAN[1], S. ALI[1] and J. T. MENDONCA[2]

[1]National Centre for Physics, Quaid-i-Azam University Campus, Islamabad 45320, Pakistan
(sakhan@ncp.edu.pk)
[2]IPFN, Instituto Superior T′echnico, Av. Rovisco Pais 1, 1049-001 Lisboa, Portugal

(Received 18 May 2013; revised 24 June 2013; accepted 24 June 2013; first published online 13 August 2013)

Abstract. The existence of plasmons with orbital angular momentum due to the Laguerre–Gaussian-type density and potential perturbations is studied in an unmagnetized quantum plasma. Starting from appropriate hydrodynamic equations for the electrostatic electron dynamics, a dispersion equation is derived in paraxial approximation. The Laguerre–Gaussian beam solutions are obtained and the properties of electric field components, energy flux, and corresponding angular momentum density of plasmons are investigated. The electric field lines are found to form helical structures with a dominant axial component. The results are analyzed numerically and the influence of radial and angular mode numbers on potential and electric field components is illustrated.

1. Introduction

The study of plasmons is a fascinating paradigm of collective electron oscillations in classical and quantum plasmas (Pines and Schrieffer 1962) leading to plasmonics – the research field currently underway at a breathtaking pace due to some ingenious applications as a result of rapid advancement in fabrication techniques and computing power (Atwater 2007; Maier 2007; Pacifici 2007). It enables the tailoring and manipulation of optical signals in matter with a footprint smaller than the wavelength of light. Recently, Glenzer et al. (Glenzer 2007; Glenzer and Redmer 2009) have employed laser-based intense X-ray sources to study the physical properties of dense degenerate plasma using Thomson scattering technique and shown that the X-ray forward scattering spectrum can be used to measure the collective plasmon oscillations consistent with the plasmon dispersion relation. Besides extracting the plasmon parameters, the authors have shown the direct measurement of collision and quantum effects. Various other properties of electron plasma oscillations in non-relativistic degenerate quantum plasmas have also been recognized by the researchers (Itoh et al. 1982; Bellac and Manuel 1997; Basagoiti 1998; Shukla and Eliasson 2007, 2008; Khan and Saleem 2009; Eliasson and Shukla 2011; Mendonca 2011), for instance, damping of plasmons, its spectral properties, plasmon localization, and dynamics, etc. In quantum plasmas, the equilibrium electron distribution follows Fermi–Dirac statistics $\propto \exp[(\varepsilon-\mu)/k_BT]^{-1}$, where ε is electron energy and μ is the chemical potential. The electron de Broglie wavelength λ_{Be} $(=h/\sqrt{2\pi m_e k_B T})$ is of the order of average interparticle distance $n_e^{-1/3}$, where m_e, n_e, and h are the electron mass, electron number density, and Planck's constant, respectively. For high density and low temperature, $\mu \to \varepsilon_{Fe}$ and $\varepsilon_{Fe}/k_BT \gtrsim 1$, where $\varepsilon_{Fe} = (\hbar^2/2m_e)(3\pi^2 n_e)^{2/3}$ is the electron Fermi energy. The ions may behave classically or quantum mechanically depending upon ion degeneracy parameter which is larger than unity for the quantum case.

Quantum hydrodynamic (QHD) description has been employed frequently in the recent years to study the degenerate quantum plasmas ranging from nanoscience (Manfredi 2005; Crouseilles et al. 2008) to lasers (Serbeto et al. 2009) and astrophysics (Haas 2005), for an overview, see Shukla and Eliasson (2011). The QHD model is capable to capture some important quantum effects such as electron Fermi degeneracy and quantum Bohm potential. Very recently, Hefferon et al. (2010) have shown that relativistic laser pulses in an X-ray regime (∼100 fs) propagating in a dense cold quantum plasma (typical densities $\gtrsim 10^{26}\mathrm{cm}^{-3}$) compress and localize to temporal sizes of attosecond, and spatial sizes of micron order. The laser-excited electrostatic wakefields can trap electrons and accelerate them to high energies at nanoscales (Shukla et al. 2009). The electron Fermi pressure and tunneling effect (Bohm potential) change the classical behavior of the electron plasma waves with wavelength of the order of electron skin depth or even shorter. It also enhances the magnetization and cyclotron motion in cold quantum plasmas due to ponderomotive force of electromagnetic pulses (Jung and Murakami 2009). For plasma densities indicated above, the plasmon decay rate is a decreasing function of electron number density even for finite electron temperature (Son et al. 2010). In other words, the plasmon damping rate is contained by electron degeneracy which, in turn, reduces the electron–ion

https://doi.org/10.1017/S0022377813000809 Published online by Cambridge University Press

collisions and bremsstrahlung (Son and Fisch 2004). The hydrodynamic studies of surface plasmons in a degenerate quantum plasma have also shown important consequences and new quantum limits in the design of plasmonic devices (Marklund et al. 2008).

The mechanical influence of light beams on matter is mostly associated with linear momentum (Stenholm 1986). It is well known that the photons carry a spin angular momentum $\pm\hbar$ when circularly polarized. It was first observed experimentally by Beth (1936) in 1935 that the exchange of angular momentum acts as a counter-torque which induces rotations on a waveplate. In circularly polarized light, photon spins are aligned resulting in a finite angular momentum. The transfer of angular momentum in light–matter interactions led to a great deal of studies for many years, however, emphasis remained on the circularly polarized light and electromagnetic modes (Jauch and Rohrlich 1976; Tannoudji et al. 1989; Hains 2001).

It has been known for long that photon beams can carry an additional angular momentum associated with its spatial distribution (Jackson 1962). About two decades ago, Allen et al. (1992) demonstrated that light beams carry an orbital angular momentum (OAM), additional and independent of photon spin. It is now recognized that collimated light beams carrying OAM can be produced in the laboratory, which has led to a wide variety of applications and many more are expected (O' Neil et al. 2002; Verbeeck et al. 2010; Padgett and Bowman 2011). Such beams can be described by Laguerre–Gaussian (LG) mode set with a well-defined OAM $l\hbar$ per photon, with l being the azimuthal mode index, which can take any integer value. The azimuthal phase component corresponds to a helical wavefront of the beam dictating a non-zero azimuthal component of the poynting vector at every radial position r in the beam. The azimuthal helical wave function of the LG modes in radial coordinates can simply be given as

$$\Psi_{LG}(r,\varphi) \propto e^{il\varphi}L(r), \tag{1}$$

where φ is the azimuthal angle, r is the radial coordinate, and $L(r)$ is a Laguerre function. Photons with helical wavefronts can be represented on the basis of orthogonal LG modes each associated with a well-defined OAM. The physical significance of the OAM of photons has been discussed in detail in different contexts, e.g. stimulated Raman and Brillouin backscattering processes (Mendonca et al. 2009b), where the existence of plasmon and phonon states with OAM was introduced for the first time. Similarly, its importance in the generation of an axial magnetic field (Ali et al. 2010), magnetization of electron–positron plasmas (Shukla and Eliasson 2010), stimulated scattering instabilities of coherent electromagnetic waves in quantum plasmas (Shukla et al. 2012), and astrophysical settings (Harwitt 2003) has been pointed out.

The plasmon response and nonlinear structures as a result of the interaction of LG light beams with matter lead to various important applications (Dienerowitz et al. 2008; Kim et al. 2010; Lembessis et al. 2011). The LG plasmons carry finite angular momentum analogous to photons since plasmons are just longitudinal photons (Mendonca et al. 2009a). In paraxial approximation, the electric field lines are not parallel straight lines for LG plasmon modes but helical, wandering around the axial direction of the plasmon beam. The magnetic field generation is usually associated with polarized radiation; however, the axial magnetic field can also be produced by LG plasmon beams in a collisionless unmagnetized homogeneous plasma (Ali and Mendonca 2011). The magnetic field increases with plasmon density or equivalently with the energy of the LG plasmon. In this letter, we investigate the properties of LG plasmon modes in a completely degenerate electron–ion plasma. It is important to note that the electrostatic modes have no spin or intrinsic angular momentum. Therefore, unlike the case of transverse wave modes or photons which possess spin as determined by their right- or left-hand polarization states, in the case of plasmons or phonons, the OAM is identical to their total angular momentum.

The letter is organized as follows. The basic model is given in Sec. 2. In Secs. 3 and 4, we describe the electric field and angular momentum density due to plasmons, whereas Sec. 5 presents the numerical analysis and summary of our results.

2. Quantum hydrodynamic equations and paraxial approximation for plasmons

Let us consider an unmagnetized homogeneous degenerate quantum plasma comprising of inertial electrons with stationary ions making a neutralizing background. To study the electrostatic electron dynamics, we employ the electron momentum conservation equation (Marklund et al. 2008):

$$m_e n_e \left(\frac{\partial}{\partial t} + \mathbf{v}_e \cdot \nabla\right)\mathbf{v}_e = -en_e\mathbf{E} - \nabla P_e + \frac{\hbar^2 n_e}{2m_e}\nabla\left(\frac{\nabla^2\sqrt{n_e}}{\sqrt{n_e}}\right), \tag{2}$$

the continuity equation $\partial_t n_e + \nabla\cdot(n_e\mathbf{v}_e) = 0$, and the Poisson equation $\nabla\cdot\mathbf{E} = 4\pi e(n_e - n_0)$, where $\mathbf{v}_e$, $\mathbf{E}$, P_e, and n_0 are the electron fluid velocity, electric field, electron pressure, and unperturbed density, respectively, where the steady state is defined as $n_{e0} = n_{i0} = n_0$. The last term in (2) is the gradient of the quantum Bohm potential which corresponds to the effect of wave function dispersion or quantum diffraction. We consider a non-relativistic degenerate electron gas, so that the electron Fermi pressure (Manfredi 2005; Marklund et al. 2008) is of most significance, as given by

$$P_{Fe} = \left(\frac{4\pi^2\hbar^2}{5m_e}\right)\left(\frac{3}{8\pi}\right)^{2/3} n_e^{5/3}. \tag{3}$$

https://doi.org/10.1017/S0022377813000809 Published online by Cambridge University Press

The linearized momentum conservation equation leads to

$$\frac{\partial \tilde{\mathbf{v}}_e}{\partial t} = -\frac{e}{m_e}\tilde{\mathbf{E}} - c_F^2 \nabla\left(\frac{\tilde{n}_e}{n_0}\right) + \frac{\hbar^2}{4m_e^2}\nabla\left[\nabla^2\left(\frac{\tilde{n}_e}{n_0}\right)\right], \quad (4)$$

where $c_F = (\frac{2\pi\hbar}{\sqrt{3}m_e})(\frac{3n_0}{8\pi})^{1/3}$ is the speed of the wave associated with degenerate electrons and tilde notation in (4) corresponds to the perturbed quantities. This further gives

$$\left[\frac{\partial^2}{\partial t^2} + \omega_{pe}^2\left(1 - \frac{c_F^2}{\omega_{pe}^2}\nabla^2 + \frac{\hbar^2}{m_e^2\omega_{pe}^2}\nabla^4\right)\right]\tilde{n}_e = 0, \quad (5)$$

with $\omega_{pe} = (4\pi n_0 e^2/m_e)^{1/2}$ being the electron plasma frequency. Assuming the perturbations $\propto \exp(i\mathbf{k}\cdot\mathbf{r} - i\omega t)$, it is easy to identify the two distinct dispersive effects associated with parameters, namely, $k^2c_F^2/\omega_{pe}^2$ in the long wavelength regime when Fermi pressure dominates over the Bohm potential, and $\hbar^2k^4/m_e^2\omega_{pe}^2$ in the short wavelength regime when Bohm potential dominates over the Fermi pressure. The electron density perturbation gives rise to the electric field which can be expressed as $\mathbf{E}(\mathbf{r},t) = -\nabla V(\mathbf{r},t)$, where V is the electrostatic potential leading to the excitation of electron plasma oscillations.

Let us consider beam-type solutions instead of plane wave solutions which carry no angular momentum. Such beam solutions can be excited by Raman scattering of intense laser pulses as considered in Mendonca et al. (2009b). The slowly varying spatial part $\tilde{n}_0(\mathbf{r})$ of such a solution $\tilde{n}_e(\mathbf{r},t) = \tilde{n}_0(\mathbf{r})\exp(ikz - i\omega t)$ describes the wave profile. We consider the Fermi pressure-dominated case by dropping the last term in parenthesis in (5), and assuming that the paraxial approximation is valid such that the transverse characteristics of the plasmon beam do not change significantly in the time scale of interest. Using $\tilde{n}_e$ in (5) and assuming $\frac{\partial^2\tilde{n}_e}{\partial z^2} \ll 2k\frac{\partial\tilde{n}_e}{\partial z}$ in the paraxial approximation similar to the case of the electromagnetic wave, we obtain the well-known paraxial equation given by

$$\left(\nabla_\perp^2 + 2ik\frac{\partial}{\partial z}\right)\tilde{n}_0(\mathbf{r}) = 0, \quad (6)$$

where cylindrical coordinates (r,φ,z) have been used to write the transverse Laplacian operator as $\nabla_\perp^2 = (1/r)\partial/\partial r(r\partial/\partial r) + (1/r^2)\partial^2/\partial\varphi^2$. The longitudinal wave number k is assumed to satisfy the linear dispersion equation for degenerate electrons, i.e. $\omega^2 = \omega_{pe}^2 + k^2c_F^2$. It is to be noted that in the laser–plasma interaction, there are regimes where the transverse distribution of laser amplitude does not change appreciably. Then, the perpendicular dimension of the problem can be ignored and paraxial approximation is a useful choice, which leads to the advantage of the simplification of the model. A similar argument is applicable to the corresponding plasmon modes (Mendonca et al. 2009b).

For better understanding of the physical significance of the paraxial approximation, we start with the simplest axially symmetric beam solution written in terms of the Gaussian function given by

$$\tilde{n}_0(\mathbf{r}) = \tilde{n}_0(r,z) = N_0(z)\exp\left(ik\frac{r^2}{2R(z)}\right), \quad (7)$$

where $r = (x^2 + y^2)^{1/2}$ is the radial coordinate, $N_0(z)$ is the maximum amplitude of the Gaussian beam, and $R(z)$ is the beam waist, which is complex in nature. Using (7) in (6), we obtain

$$\left[\frac{k^2r^2}{R^2}\left(\frac{dR}{dz} - 1\right) + 2ik\left(\frac{1}{R} + \frac{1}{N_0}\frac{dN_0}{dz}\right)\right]\tilde{n}_0(\mathbf{r}) = 0, \quad (8)$$

which satisfy the boundary conditions

$$R(z) = R_0 + z - z_0, \quad \text{and} \quad N_0(z) = \frac{N_0(0)R_0}{R(z)} \equiv \frac{N_0(0)}{1 + (z - z_0)/R_0}, \quad (9)$$

where R_0 is the minimum electrostatic beam waist and $N_0(0)$ is the maximum wave amplitude at the focal position $z = z_0$.

The electrostatic paraxial equation (6) is analogous to the electromagnetic paraxial equation, whose solution can be given in terms of LG functions. The LG functions form a set of orthogonal and normalizable functions in the (r,φ) plane each of which can be expressed as

$$\tilde{n}_0(r,\varphi,z) = \tilde{N}_0 F_{pl}(r,z)\exp(il\varphi). \quad (10)$$

Here, p and l are the radial and angular mode numbers, respectively, and φ is the azimuthal angle. In (10), $F_{pl}(r,z)$ is the LG function given by

$$F_{pl}(r,z) = \frac{1}{2\sqrt{\pi}}\left(\sqrt{\frac{(|l|+p)!}{p!}}\right)x^{|l|}L_p^{|l|}(x)\exp(-x/2), \quad (11)$$

where $x = r^2/w^2(z)$, $w(z)$ is the beam waist, and $L_p^{|l|}(x)$ is the associated Laguerre polynomial defined by the Rodrigues formula as follows:

$$L_p^{|l|}(x) = \frac{\exp(x)\,x^{-|l|}}{p!}\frac{d^p}{dx^p}[x^{|l|+p}\exp(-x)]. \quad (12)$$

For $l = 0, p = 0$, and $R(z) = -ikw^2(z)$, and the Gaussian solution (7) is recovered as expected.

3. Electrostatic potential and electric field components

We now consider the electric field corresponding to the solution found in the previous section to reveal the characteristics of the plasmons. The electrostatic potential can be associated with the LG density perturbation (10) through the potential equation

$$\nabla^2 V = 4\pi e\tilde{n}_e, \quad (13)$$

where the electrostatic field $E(r,t) = -\nabla V$. Assuming the potential function of the same form as the electron density perturbation, one can write

$$V(\mathbf{r},t) = V_{pl}(r,z)\exp(il\varphi)\exp(ikz - i\omega t), \quad (14)$$

https://doi.org/10.1017/S0022377813000809 Published online by Cambridge University Press

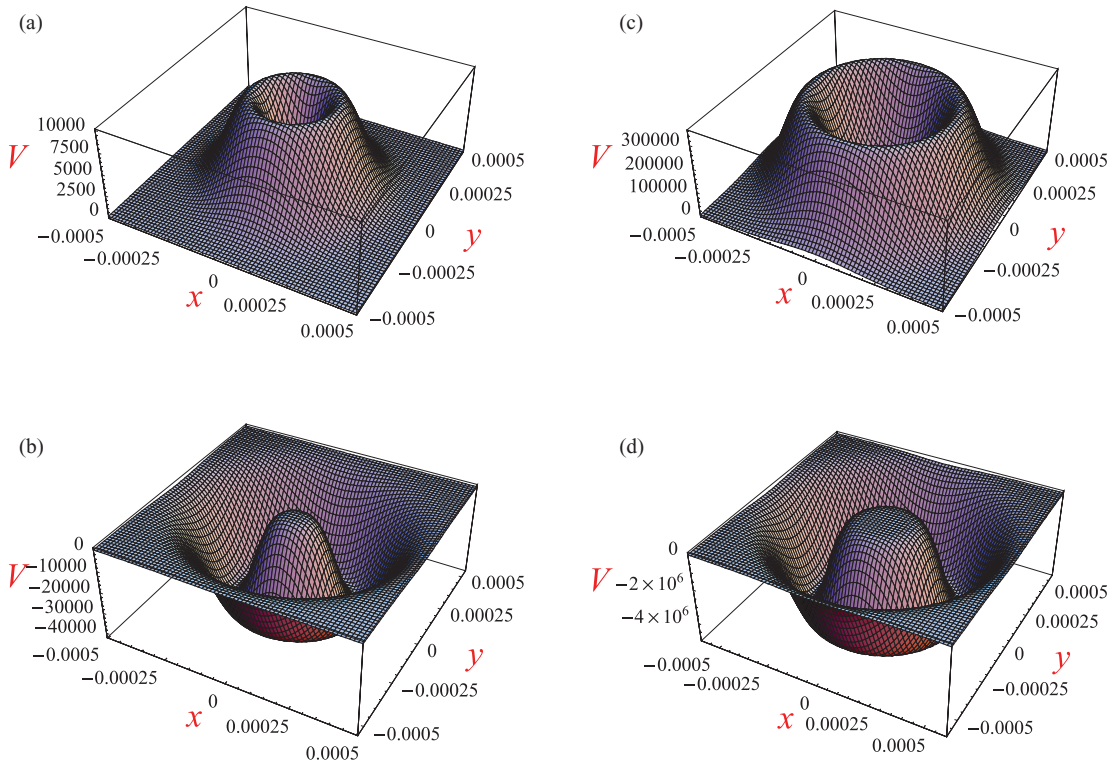


Figure 1. (Colour online) Spatial profile of the LG potential from (16) is shown at $t = 0$ with the angular mode number l keeping the radial index fixed ($p = 0$). The upper panel represents odd numbers: (a) $l = 1$, (c) $l = 3$; and the lower panel represents even numbers: (b) $l = 2$ and (d) $l = 4$, where $\varphi = \pi$.

where (13) evolves into the equation

$$\left(\nabla_{\perp}^2 + 2ik\frac{\partial}{\partial z} - k^2\right) V = 4\pi e\tilde{n}_e. \tag{15}$$

In paraxial approximation, V is described by the LG function, and we can write $V_{pl}(r,z) = \tilde{V}_0 F_{pl}(r,z)$. Then, (15) reduces to $k^2 V = -4\pi e\tilde{n}_e$. It gives the amplitude of LG potential perturbation in terms of the assumed LG density perturbation $\tilde{V}_0 = -4\pi e\tilde{N}_0/k^2$. So, the electrostatic potential for the LG mode consistent with the existence of finite OAM will be of the form

$$V(\mathbf{r},t) = \tilde{V}_0 F_{pl}(r,z)\exp(il\varphi)\exp(ikz - i\omega t). \tag{16}$$

Then, the components of the electrostatic field in cylindrical coordinates can be written as

$$E_r = -\frac{\partial V}{\partial r} \equiv -\frac{1}{F_{pl}}\frac{\partial F_{pl}}{\partial r}V, \tag{17}$$

$$E_\varphi = -\frac{1}{r}\frac{\partial V}{\partial \varphi} \equiv -\frac{il}{r}V, \tag{18}$$

and

$$E_z = -\frac{\partial V}{\partial z} \equiv -\left(ik + \frac{1}{F_{pl}}\frac{\partial F_{pl}}{\partial z}\right)V. \tag{19}$$

It is seen from the foregoing equations that the electric field lines are not straight lines along the z direction as in ordinary plane wave solutions but are showing helical structures with the radial and polar components. However, the axial component of the field is still dominant. This is in accordance with the paraxial approximation used to derive (6), whose solution is given in terms of LG functions. The LG potential perturbations arising due to LG density fluctuations of electrons give rise to the existence of electric field components (17)–(19) and the unusual shape of plasmon mode.

4. Angular momentum density

Now, we will demonstrate that the LG plasmon modes of degenerate plasma carry a finite OAM. The flux of the energy associated with this electrostatic mode can be determined in the same sense as that of the electromagnetic energy given by the relation (Stix 1992)

$$\mathbf{T} = W\mathbf{v}_g, \tag{20}$$

where $\mathbf{v}_g = v_g\hat{\mathbf{e}}_{ef}$ is the group velocity given by

$$v_g = \frac{c_F k\lambda_F}{\left(1+\lambda_F^2 k^2\right)^{1/2}}, \tag{21}$$

$\hat{\mathbf{e}}_{ef}(=\mathbf{k}_{ef}/k_{ef})$ is the unit vector parallel to the electric field of the wave and $\lambda_F = c_F/\omega_{pe}$. For $k^2\lambda_F^2 \ll 1$, $v_g \cong c_F k\lambda_F$. Generally, the energy density depends upon the electric and magnetic potentials. However, in the case of plasmons, the energy flux (20) contains the electrostatic part only. The energy density (W) associated with plasmon mode can be expressed taking into account the

https://doi.org/10.1017/S0022377813000809 Published online by Cambridge University Press

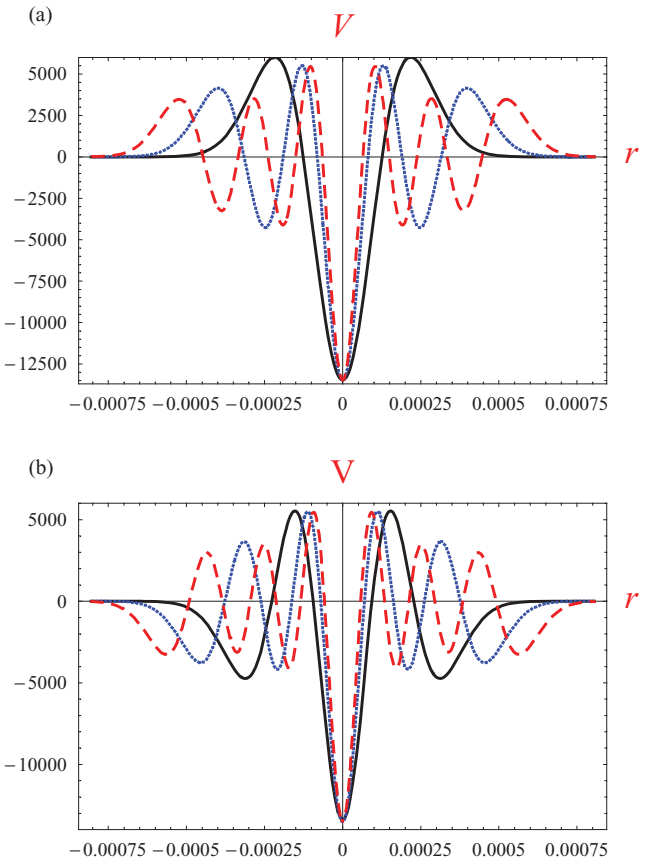


Figure 2. (Colour online) The LG potential V (statvolt) is plotted versus r (cm) for odd and even radial indices. The upper panel (a) corresponds to odd indices and the lower panel (b) to even indices, represented by solid ($p = 1, 2$), dotted ($p = 3, 4$), and dashed ($p = 5, 6$) lines, respectively, where $l = 0$ and $\varphi = \pi$.

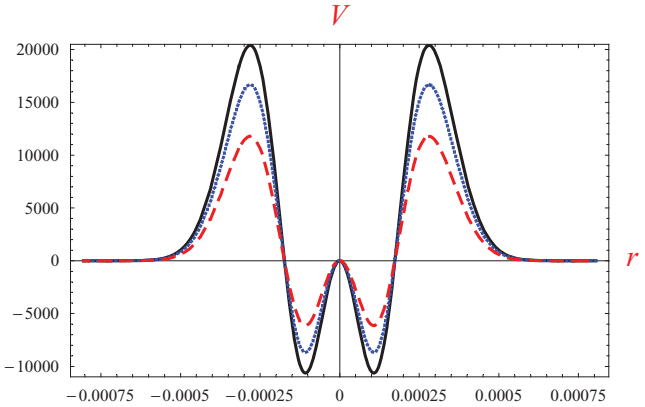


Figure 3. (Colour online) Amplitude variation of V (statvolt) with r (cm) for different values of azimuthal angle. The solid (dotted) line represents $\varphi = \pi/6$ ($\pi/4$) and the dashed line represents $\varphi = \pi/3$, where $l = p = 1$.

dispersive character of the medium, as

$$W = \frac{|E|^2}{8\pi}\left(1 + \omega_{pe}^2 \frac{\omega^2 + k^2 c_F^2}{\left(\omega^2 - k^2 c_F^2\right)^2}\right), \tag{22}$$

with $|E|^2 = \mathbf{E}\cdot\mathbf{E}^*$ being the average electrostatic energy, and the second term in parenthesis being the portion of the charged particle energy associated with coherent wave motion. The time-averaged angular momentum density in cylindrical coordinates can be given, by definition, as

$$\mathbf{M}(\mathbf{r}) = \mathbf{r} \times \langle \mathbf{P} \rangle, \tag{23}$$

where $\langle \mathbf{P} \rangle = \langle \mathbf{T} \rangle / v_g^2$. The axial component of the angular momentum density M_z along the direction of the propagation of the beam is of particular importance. It is proportional to the angular mode number l just like transverse photons. So, M_z can be expressed as

$$M_z = \frac{l}{8\pi v_g}\left(1 + \omega_{pe}^2 \frac{\omega^2 + k^2 c_F^2}{\left(\omega^2 - k^2 c_F^2\right)^2}\right) |k_{ef}| \left\langle |V(r, \varphi, t)|^2 \right\rangle. \tag{24}$$

It is to be noted that for $l = 0$, $M_z \to 0$. It means that a pure Gaussian beam with no angular structure will have no angular momentum in quantum plasmas, and angular momentum density will exist only when $l \neq 0$.

5. Discussions and summary

In this section, we examine the results numerically by using the parameters consistent with plasmon modes in quantum plasmas (Marklund et al. 2008). Scattering experiments have demonstrated that electron densities $\sim 10^{24}$ cm^{-3}, and even hundred times higher will become possible in future inertial confinement fusion experiments (Glenzer and Redmer 2009). The temporal and spatial scale lengths become very short in such high-density plasmas (Hefferon et al. 2010). It is notable that the resolvable length scales in QHD are large in general ($l >$ several $\bar{r}$; $\bar{r} \sim n_0^{-1/3}$), which means that the applicability of the model demands large wavelengths $\lambda \gg \lambda_F$. For densities $\sim 10^{26}$ cm^{-3}, $\lambda_F \sim 10^{-9}$ cm. We have considered the typical parameters: $n_0 = 1 \times 10^{26}$ cm^{-3}, $N_0 \sim 0.1 n_0$,and the beam waist $w_0 = 20\lambda$, where λ $(= 2\pi/k)$ is the wavelength of plasmon mode with $k = 1 \times 10^6$ cm^{-1} within the QHD limit ($k\lambda_F \ll 1$). The spatial profile of the scalar potential $V(r)$ associated with LG plasmon modes is plotted in Fig. 1 as a function of r, for a fixed radial mode number ($p = 0$), at $t = 0$, $z = 0$, and $\varphi = \pi$. We have found a three-dimensional view of the LG potential for different values (even and odd) of angular mode numbers l. It is seen that the amplitude of the LG potential increases with l, and odd (even) values of l lead to the positive (negative) LG potential. We have also obtained the LG potential profile with the variation of the radial mode number p as shown in Fig. 2. The increase in p enhances the node numbers whereas the amplitude (width) of $V(r)$ remains constant (decreases) with p. The curve is symmetrical on both sides of the vertical axis. The variation of the LG potential for different values of the azimuthal angle is shown in Fig. 3 with the radial and angular mode numbers fixed ($p = 0, l = 0$). It is found that the amplitude of $V(r)$ decreases with φ. Figure 4 displays a

https://doi.org/10.1017/S0022377813000809 Published online by Cambridge University Press

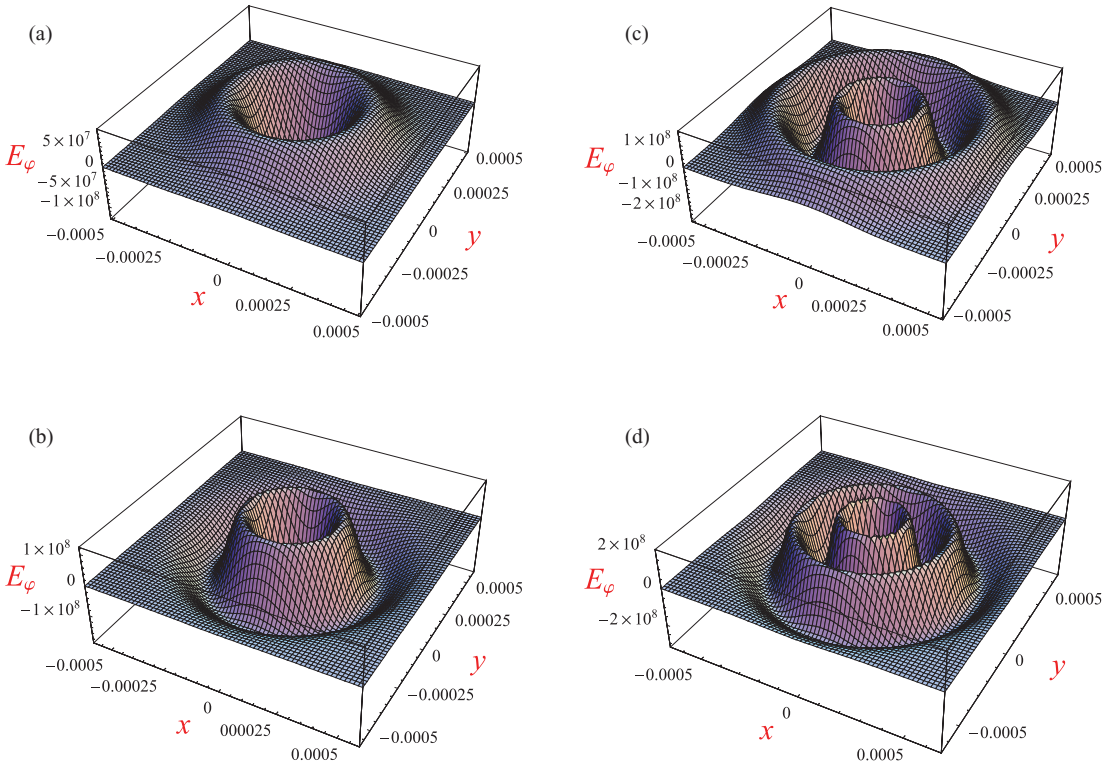


Figure 4. (Colour online) The azimuthal component of the electric field E_φ (statvolt cm^{-1}) is plotted against the radial distance r (cm) with the variation of the radial index p. In the upper (lower) panel, even (odd) values of p are given with (a) $p = 1$, (b) $p = 2$, (c) $p = 3$, and (d) $p = 4$, where $l = 1$ and $\varphi = \pi/2$.

three-dimensional image of the azimuthal component of the electric field keeping the angular mode number fixed and varying the radial mode number ($p = 1, 2, 3, 4$). It is noted that the amplitude of the electric field strongly depends on the value of p as expected, which can also be useful for the generation of an axial magnetic field due to plasmons (Ali et al. 2010) in quantum plasmas. The oscillations seem like the electron plasma waves with a transverse structure, which can be considered analogous to the electromagnetic wave mode, and LG-type density and potential perturbations contribute to the OAM of such modes.

To summarize, we have investigated the LG plasmon mode in a strongly degenerate quantum plasma. A linear equation in paraxial approximation for electron density perturbations is derived and Gaussian beam solutions as well as more general LG solutions are considered. The potential equation is solved for LG potential perturbations, and the electric field components, energy flux, and the corresponding angular momentum density of plasmons are investigated. It shows that the electric field lines are helical structures instead of straight lines, and the LG plasmon modes have a finite value of the axial angular momentum proportional to the angular mode number. In contrast to the photon beam case, plasmons have no spin, and the plasmon angular momentum is the same as the total angular momentum. In this direction, a more general study can be carried out with different geometrical and physical conditions, which will be addressed in some future work.

References

Ali, S., Davies, J. R. and Mendonca, J. T. 2010 *Phys. Rev. Lett.* **105**, 035001.

Ali, S. and Mendonca, J. T. 2011 *Plasma Phys. Control. Fusion* **53**, 045007.

Allen, L. et al. 1992 *Phys. Rev.* A **45**, 8185.

Atwater, H. A. 2007 *Sci. Am.* **296**, 56.

Basagoiti, M. A. V. 1998 *Phys. Rev.* D **57**, 7618.

Bellac, M. L. and Manuel, C. 1997 *Phys. Rev.* D **55**, 3215.

Beth, R. A. 1936 *Rev. Mod. Phys.* **50**, 115.

Crouseilles, N., Hervieux. P.-A. and Manfredi, G. 2008 *Phys. Rev.* B **78**, 155412.

Dienerowitz, M., Mazilu, M. and Dholakia, K. 2008 *J. Nanophoton.* **2**, 021875.

Eliasson, B. and Shukla, P. K. 2011 *Phys. Rev.* E **83**, 046407.

Glenzer, S. H. 2007 *AIP Conf. Proc.* **926**, 8.

Glenzer, S. H. and Redmer R. 2009 *Rev. Mod. Phys.* **81**, 1625.

Haas, F. 2005 *Phys. Plasmas* **12**, 062117.

Hains, M. G. 2001 *Phys. Rev. Lett.* **87,** 135005.

Harwitt, M. 2003 *Astrophys. J.* **597**, 1266.

Hefferon, G., Sharma, A. and Kourakis, I. 2010 *Phys. Lett.* A **374**, 4336.

Itoh, N. et al. 1982 *Phys. Rev. Lett.* **49**, 1932.

Jackson, J. D. 1962 *Classical Electrodynamics*, 2nd edn. New York: Wiley.

Jauch, J. M. and Rohrlich, F. 1976 *The Theory of Photons and Electrons.* Berlin: Springer-Verlag.

Jung, Y.-D. and Murakami, I. 2009 *Phys. Lett.* A **373**, 969.

Khan, S. A. and Saleem, H. 2009 *Phys. Plasmas* **16**, 052109.

Kim, H. et al. 2010 *Nano Lett.* **10**, 529.

Lembessis, V. E. et al. 2011 *J. Opt.* **13**, 064002.

https://doi.org/10.1017/S0022377813000809 Published online by Cambridge University Press

Maier, S. A. 2007 *Plasmonics: Fundamentals and Applications.* New York: Springer-Verlag.

Manfredi, G. 2005 *Fields Inst. Commun.* **46**, 263.

Marklund, M. et al. 2008 *Euro. Phys. Lett.* **84**, 17006.

Mendonca, J. T. 2011 *Phys. Plasma* **18**, 062101.

Mendonca, J. T., Ali, S. and Thide, B. 2009a *Phys. Plasma* **16**, 112103.

Mendonca, J .T., Thide, B. and Then, U. 2009b *Phys. Rev. Lett.* **102**, 185005.

O' Neil, A. T. et al. 2002 *Phys. Rev. Lett.* **88**, 053601.

Pacifici, D. 2007 *Nature Photon.* **1**, 689.

Padgett, M. and Bowman, R. 2011 *Nature Photon.* **5**, 343.

Pines, D. and Schrieffer, J. R. 1962 *Phys. Rev.* **125**, 804.

Serbeto, A. et al. 2009 *Plasma Phys. Control. Fusion* **51**, 124024.

Shukla, P. K. and Eliasson, B. 2007 *Phys. Lett.* A **372**, 2893.

Shukla, P. K. and Eliasson, B. 2008 *Phys. Lett.* A **372**, 2897.

Shukla, P. K. and Eliasson, B. 2010 *J. Plasma Phys.* **76**, 887.

Shukla, P. K. and Eliasson, B. 2011 *Rev. Mod. Phys.* **83**, 885.

Shukla, P. K., Eliasson, B. and Stenflo, L. 2012 *Phys. Rev.* E **86**, 016403.

Shukla, P. K. et al. 2009 *Phys. Lett.* A **373,** 3165.

Son, S. and Fisch, N. J. 2004 *Phys. Lett.* A **329**, 76.

Son, S., Ku, S. and Moon, S. J. 2010 *Phys. Plasmas* **17**, 112709.

Stenholm, S. 1986 *Rev. Mod. Phys.* **58**, 699.

Stix, T. H. 1992 *Waves in Plasmas.* New York: American Institute of Physics.

Tannoudji, C. C., Dupont-Roc, J. and Grynberg, G. 1989 *Photons and Atoms.* New York: Wiley.

Verbeeck, J., Tian, H. and Schattschneider, P. 2010 *Nature* **467**, 301.

https://doi.org/10.1017/S0022377813000809 Published online by Cambridge University Press